ELSEVIER

Astroparticle Physics 3 (1995) 1–15

Astroparticle Physics

Results on candidate UHE gamma-ray sources by the EAS-TOP array (1989–1993)

M. Aglietta [a,b], B. Alessandro [b], P. Antonioli [b,c], F. Arneodo [d], L. Bergamasco [b,c], A. Campos Fauth [e], C. Castagnoli [a,b], A. Castellina [a,b], A. Chiavassa [b,c], G. Cini [b,c], B. D'Ettorre Piazzoli [f], G. Di Sciascio [f], W. Fulgione [a,b], P. Galeotti [b,c], P.L. Ghia [a,b], M. Iacovacci [f], G. Mannocchi [a,b], C. Morello [a,b], G. Navarra [b,c,*], L. Riccati [b], O. Saavedra [b,c], G.C. Trinchero [a,b], P. Vallania [a,b], S. Vernetto [a,b]

[a] *Istituto di Cosmo-Geofisica del CNR, Corso Fiume 4, 10133, Torino, Italy*
[b] *Istituto Nazionale di Fisica Nucleare, Sezione di Torino, Via Pietro Giuria 1, 10125, Torino, Italy*
[c] *Istituto di Fisica dell' Università, Via Pietro Giuria 1, 10125, Torino, Italy*
[d] *Dipartimento di Fisica dell' Università, Via Vetoio, 67010, Coppito, L'Aquila, Italy*
[e] *Instituto di Fisica, Universidade Estadual de Campinas, Cidade Universitaria "Zeferino Vaz", Barao Geraldo, 13081, Campinas, Brazil*
[f] *Dipartimento di Scienze Fisiche dell' Università di Napoli and INFN, Mostra D'Oltremare, Pad. 20, 80125, Napoli, Italy*

Received 14 June 1994; in final form 18 August 1994

Abstract

A search for UHE gamma-rays from 13 candidate point sources observable in the northern hemisphere (the Crab Nebula and Pulsar, Cygnus X-3, Hercules X-1, Geminga and others) has been performed by the EAS-TOP array during four years of operation since January 1989 to December 1993, at different energy thresholds ($E_0 = 30$–300 TeV). DC, periodic and sporadic emissions have been studied, and no evidence for significant excesses has been found from any of these searches. The derived 90% c.l. upper limits to the d.c. flux, for a source culminating at the zenith such as Cygnus X-3, are $\Phi(E > 230\ \text{TeV}) < 2 \times 10^{-14}\ \text{cm}^{-2}\ \text{s}^{-1}$, $\Phi(E > 90\ \text{TeV}) < 4.1 \times 10^{-14}\ \text{cm}^{-2}\ \text{s}^{-1}$ and $\Phi(E > 25\ \text{TeV}) < 1.9 \times 10^{-13}\ \text{cm}^{-2}\ \text{s}^{-1}$. The excess from the Crab Nebula of February 23, 1989, as reported by the EAS-TOP, Baksan and KGF arrays, remains the only sporadic excess detected with statistically significant confidence level (probability of background imitation $\approx 10^{-5}$).

1. Introduction

The search for gamma-ray emission from point sources at TeV and PeV energies is the main tool for understanding, together with the physics of specific stellar objects, the processes of particle acceleration and therefore the origin of high energy cosmic rays.

Among the motivations supporting the need of new measurements we remind:

– In late seventies and early eighties several groups reported gamma-ray emission from the X-ray binary system Cygnus X-3 at Very High

* Corresponding author.

SSDI 0927-6505(94)00026-3

Energy [1] ($E \geq$ TeV) and Ultra High Energy [2–4] ($E \geq 10$–100 TeV). These positive results have not been confirmed by subsequent measurements, rising the problem of their statistical significance and/or source variability.

– A significant result has been obtained by the Whipple collaboration [5] with the detection of TeV gamma-rays from the Crab Nebula. The extension of the measurement to UHE is expected to provide data on the maximum energies achieved by the pulsar acceleration mechanisms. Moreover, the possibility of sporadic emission from the Crab Nebula at UHE has been supported by the contemporaneous observation of the burst on 23 February 1989 by three different detectors (Baksan [6], KGF [7] and EAS-TOP [8]), with good confidence level.

– In the High Energy region (20 MeV $< E <$ 20 GeV), the EGRET telescope aboard GRO has extended the class of gamma-ray sources, e.g. by the discovery of the emission from Active Galactic Nuclei [9], and has improved previous knowledge, as for example by the identification of Geminga with a gamma-ray pulsar [10]. Following such observation, two groups [11,12] have reported pulsed TeV emission from Geminga in 1983 and 1984–85 databases, while the Whipple collaboration [13] has set upper limits both to steady and pulsed fluxes. Relating to AGNs, it is recent the observation of TeV gamma-ray emission from Markarian 421 [14].

It is therefore important to perform long lasting systematic measurements at UHE in order (a) to extend the knowledge of the VHE spectra, (b) to study possible long term variations, (c) to investigate phenomena of episodic emission.

This energy range ($E > 10$–100 TeV) can be explored only by means of ground based detectors, i.e. Extensive Air Shower arrays. For such measurements, the main experimental problems are due to the cosmic ray background (given the difficulties of discriminating gamma-rays from charged primaries), the limited angular resolution, and the usually poor statistics.

The EAS-TOP detector [15–16] has been developed in order to improve: (a) the collecting area ($\approx 10^5$ m^2); (b) the angular resolution ($\sigma_\vartheta <$ 1°); (c) the energy range of operation, by performing contemporaneous TeV and PeV observations at the same site (with further possibility of energy discrimination above 30 TeV); (d) the rejection power against hadronic background (through the contemporaneous detection of the e.m., muonic and hadronic components of EAS at PeV energies). The e.m. detector has been in operation since the beginning of 1989, for a total, at now, of four full years of operation and $\approx 3 \times 10^9$ collected air showers.

We present here the results of an analysis comprehensive of all the events collected between 1989 and 1993 by the e.m. detector, without any further selection criterium. Results from partial periods of measurement have already been reported, concerning candidate point sources [17–19], transients [8] and an all-sky survey [20]; furthermore a study on the diffuse galactic component has been published in Ref. [21].

Recently, results on candidate sources have been reported by other collaborations (see e.g. Refs. [22–25]).

2. The detector

The EAS-TOP Extensive Air Shower array is located at Campo Imperatore (2005 m a.s.l., lat. 42°27′N, long. 13°34′E, Gran Sasso Laboratories). The electromagnetic detector has been in operation since January 1989 under different configurations, being progressively enlarged: in Fig. 1 a scheme of the full array is shown, while in Table 1 the different phases are summarized.

At present the detector consists of 35 modules of scintillation counters (10 m^2 each, spread over an area $\geq 10^5$ m^2). The trigger is provided by any coincidence of four adjacent modules (threshold ≈ 0.3 minimum ionizing particles/module), the rate being ≈ 35 Hz. The absolute arrival time of each event is measured with a precision of 100 μs through a rubidium clock synchronized with the standard time provided by the Italian national broadcasting company.

While the experiment and the data processing have been described in detail elsewhere [16], the relevant features for gamma-ray astronomy will be outlined here.

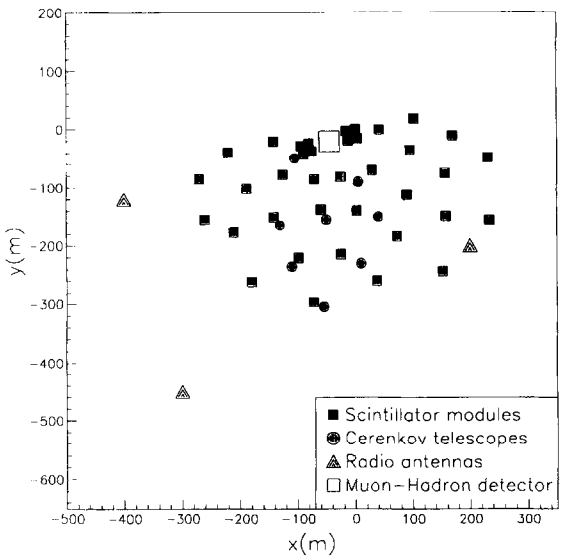

Fig. 1. Schematic view of the full EAS-TOP array.

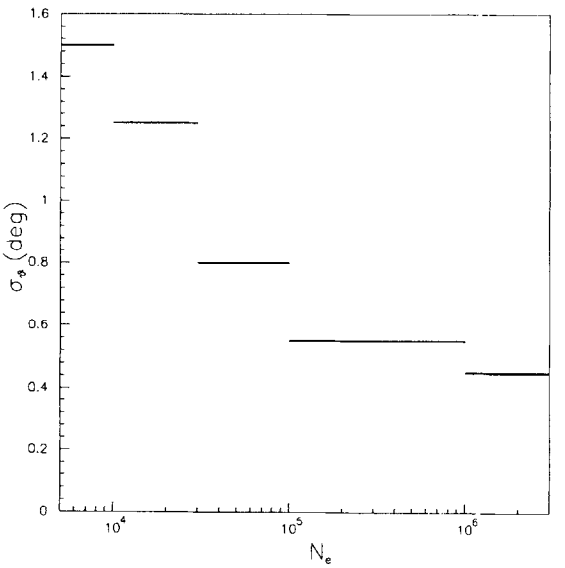

Fig. 2. The angular resolution as a function of EAS electron size N_e.

Different selection criteria are applied to the data in order to investigate different primary energies and to optimize the angular resolution; the so obtained classes of events are the following:

– S_1: at least 7 (or 6) neighbouring detectors fired, with the maximum number of particles detected by an inner module (i.e. internal events, rate $f \approx 2$ Hz in the present configuration). The arrival directions are obtained through the times of flight among the detectors located around the EAS core. The angular resolution σ_ϑ is measured by comparing, for each shower, the arrival directions obtained from two independent sets of modules: σ_ϑ is shown in Fig. 2, as a function of the shower size N_e. The measurement [26] of the shape of the Moon shadow on the flux of primary cosmic rays in each successive year of data confirms the angular resolution and provides a check of the absolute pointing of the array and of its stability. Such a measurement is performed by comparing the number of events recorded within a cone of increasing aperture centered on the Moon, with the average number of counts recorded from two analogous cones located at distances $\Delta\alpha = 1.6°$. In Fig. 3 the behavior of the percentage integral deficit of events versus the opening angle from the center of the Moon is shown, both for each year and for the global

Table 1
The different configurations of the EAS-TOP array

Epoch	Scintillator area [m^2]	Enclosed area (A_0) [m^2]	Trigger condition	Trigger rate [Hz]
Feb.–Sep. 1989	240	8.0×10^4 (4.2×10^4)	seven-fold	6
Oct. 1989–Dec. 1990 Nov. 1991–Oct. 1992	290	1.0×10^5 (5.0×10^4)	four-fold	30
Nov. 1992–present	350	1.5×10^5 (6.7×10^4)	four-fold	35

database. The total observed deficit has a significance of 4.1 s.d. and, inside 1.25°, it amounts to 332.5 events out of 4426.5 background ones. This deficit (7.5%) corresponds to the absorption of a flux of 1.4×10^{-13} cm^{-2} s^{-1}, in 1057 hours of observation at an average zenith angle $\vartheta \approx 31.5°$. Assuming a Gaussian shape for the detector point spread function ($F(\vartheta) \propto \exp(-\vartheta^2/\sigma_\vartheta^2)$), the best fit to the data of Fig. 3 is obtained with a s.d. $\sigma_\vartheta = 0.97 \pm 0.11°$. Converting this value to the vertical, we obtain $\sigma_\vartheta = 0.83 \pm 0.1°$, which represents the angular resolution with systematic effects included.

For internal events, the shower size N_e is also reconstructed, by means of a fit of the particle densities recorded by the individual detectors; the accuracy in the reconstruction of the shower size is $\Delta N_e/N_e < 0.2$ for $N_e > 10^5$.

– S_2: a subset of S_1, with the additional selection $N_e > 10^5$, for which $\sigma_\vartheta = 0.5°$ (see Fig. 2) and $f \approx 0.3$ Hz;

– S_3: at least five detectors fired (i.e. low energy internal events, or events with core location outside or at the edges of the array): σ_ϑ is $\approx 2.5°$ and $f \approx 15$ Hz;

– S_4: only four detectors fired (i.e. the minimum trigger configuration): $\sigma_\vartheta \approx 5.6°$ and $f \approx 5$ Hz.

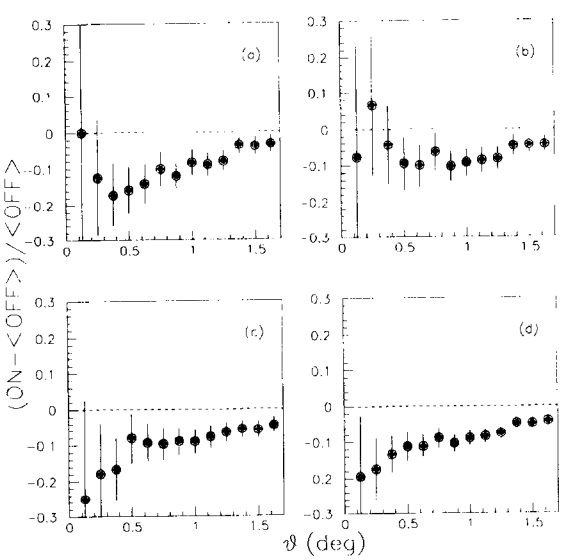

Fig. 3. Percentage integral deficit of events inside the opening angle ϑ from the center of the Moon: (a) 1990 data, (b) 1992 data, (c) 1993 data, (d) total data set.

Table 2
Characteristics of the different classes of events used in the present analysis

Events class	S_1	S_2	S_3	S_4
σ_ϑ	0.85°	0.5°	2.5°	5.6°
$\Delta\delta$	1.5°	0.8°	4.0°	4.0° [a]
angular efficiency (ϵ)	0.9	0.8	0.8	0.3

[a] To limit the time interval between ON and OFF observations this is not optimized.

The characteristics of the different classes of events are listed in Table 2.

3. The analysis

The analysis is performed by searching for statistically significant excesses in the number of counts inside a bin of dimensions optimized on the angular resolution, centered on the source (ON), with respect to six analogous background bins (OFF) (the statistical significances of the excesses are calculated following Ref. [27]). The dimensions of the bins are $\Delta\delta = 1.58\sigma_\vartheta$ and $\Delta\alpha = \Delta\delta/\cos\delta$ (see Table 2 for the values of the bin size in δ), being 1.58 the factor which maximizes the ratio of the signal to the background fluctuations in case of a Gaussian angular resolution with r.m.s. σ_ϑ. The OFF bins are located at the same declination of the source cell (ON) and shifted in right ascension of $\pm 2K\Delta\alpha$ ($K = 1, 3$). Only days in which all the seven cells are observed without interruptions up to the zenith angle $\vartheta = 40°$ are used for the analysis.

3.1. The cosmic ray background measurement and its stability

The cosmic ray flux has to be measured and monitored since it is the source of the counting rate background. Moreover, this measurement provides a test of the response of the detector to the UHE atmospheric showers and of its stability, and partially allows to overcome the problem of the absolute calibration, which is not possible for

Table 3
List of the candidate sources and of their observation parameters

Source	Min. zenith distance [deg]	$\langle\vartheta\rangle_{obs}$ [deg]	Daily exposure [h]	E_{th} [TeV] [a]	
Cygnus X-3	1.5	20.3	7.3	S_1:	90
				S_2:	230
				S_{3+4}:	25
Hercules X-1	7.1	21.7	6.9	S_1:	90
				S_2:	240
				S_{3+4}:	25
Cygnus X-1	7.2	21.7	7.0	S_1:	90
				S_2:	240
				S_{3+4}:	25
4U0115+6112	21.3	28.5	8.0	S_1:	120
				S_2:	300
				S_{3+4}:	25
Crab Nebula	20.4	28.0	5.5	S_1:	105
				S_2:	280
				S_{3+4}:	25
Geminga	24.7	30.4	5.0	S_1:	140
				S_2:	350
				S_{3+4}:	40
PSR1953+29	13.3	24.2	6.3	S_1:	100
				S_2:	260
				S_{3+4}:	25
PSR1937+214	20.9	28.1	5.5	S_1:	120
				S_2:	300
				S_{3+4}:	25
PSR0157+6112	19.9	27.7	8.0	S_1:	120
				S_2:	300
				S_{3+4}:	25
LSI+61	18.7	27.1	8.0	S_1:	120
				S_2:	300
				S_{3+4}:	25
North Gal. Pole	15.3	25.2	6.0	S_1:	100
				S_2:	260
				S_{3+4}:	25
M31	1.2	20.3	7.3	S_1:	90
				S_2:	230
				S_{3+4}:	25
Markarian 421	4.3	21.0	7.0	S_1:	90
				S_2:	240
				S_{3+4}:	25

[a] Differences in E_{th} less than 5 TeV are not considered significant.

EAS arrays. We therefore compare the EAS size spectrum measured by EAS-TOP with the one expected from the extrapolations of the direct balloon and satellite measurements at TeV energies. The interaction and cascade model of Ref. [28] is used for the conversion of E_0 to N_e. Up to the steepening of the primary spectrum (where the comparison is possible) the experimental data agree with the expectations [29]. This proves, as a first approximation, that the behavior of the detector is correct and that the calculations of the response of the array to different primary energies and of the effective areas (see Section 3.2) are reliable.

The above described procedure of background measurement for each source ensures that the ON and OFF bins are observed for the same exposure time and at the same zenith angles. Moreover, the closeness in time of such observations (within ± 1 h) compensates for smooth variations of the experimental and atmospheric conditions during the transit of the source. A conservative upper limit to possible residual effects can be obtained from the comparison between the number of counts in the two farthest OFF bins, for each source and for each class of events. All such observed differences are within 2 s.d. Poissonian fluctuations: the upper limit to not compensated instabilities, obtained from the class of events with higher statistics ($> 10^6$ events), is 8×10^{-4}. The negligible level of non-Poissonian fluctuations can also be inferred from the absence of deviations in the distributions of the sources daily excesses with respect to the statistical ones (see e.g. Figs. 6, 8, 10, 11).

3.2. *Effective areas and energy thresholds*

The array effective area $A(E)$ for each source as a function of the primary gamma-ray energy E is calculated through a simulation which includes:

- the longitudinal e.m. cascade development in the atmosphere and its fluctuations;
- the lateral distribution function according to the Nishimura–Kamata–Greisen formalism [30], which fits the experimental data;
- the transition effect in the scintillators and their containers;

– the path of each source in the sky.

In the case of events S_1 and S_2 (i.e. internal), $A(E)$ saturates at a value $A_{\text{eff}} = A_0 \cos\langle\vartheta\rangle_{\text{obs}}$ (A_0 is shown in Table 1 and $\langle\vartheta\rangle_{\text{obs}}$, for each source, in Table 3). The energy threshold E_{0i} is consequently defined as:

$$\int_0^\infty E^{-\gamma} A(E)\, \mathrm{d}E = A_{\text{eff}} \int_{E_{0i}}^\infty E^{-\gamma}\, \mathrm{d}E$$

γ being the assumed index of the differential source spectrum.

The definition of E_{0i} is then based on the geometrical area of the array. This is not possible for events S_3 and S_4 (i.e. external and low energy), for which $A(E)$ is an increasing function of E, and we define the energy threshold E_{0e} as the mode of the distribution $A(E) \cdot E^{-\gamma}$. As a first approximation, the coherence of such definition of E_{0e} is shown by the fact that the ratio E_{0e}/E_{0i} is ≈ 0.3, which reflects the ratio of the average number of detectors fired (6:14) in the two different trigger conditions.

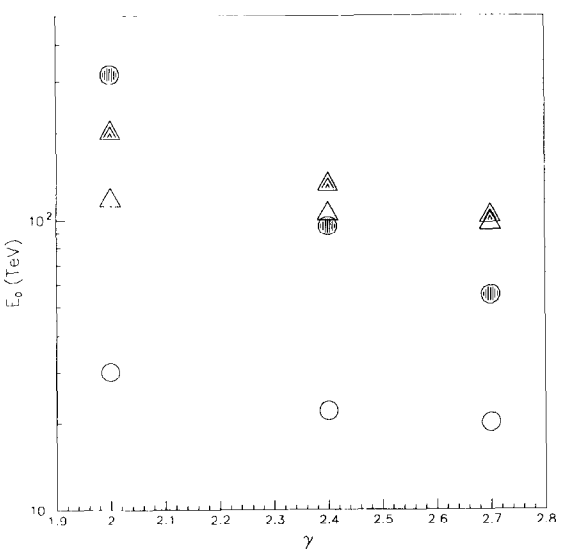

Fig. 4. Behavior of different definitions of the energy thresholds versus the differential spectrum index γ, for the case of Crab Nebula. Triangles refer to internal events, circles to external and low energy ones: the open symbols represent the values of E_{0i} and E_{0e} used in this analysis (see text for the definitions), the full symbols represent the median energies.

Since, for calculating the fluxes or the upper limits, a source spectrum ($\propto E^{-\gamma}$) has to be assumed, the stability of the energy threshold versus the assumed spectral index has to be checked. The behavior of E_{0i} and E_{0e} versus γ is shown in Fig. 4 (for the Crab Nebula): we see that in both cases such dependence is rather weak ($\Delta E_0/E_0 < 20\%$ for $\Delta\gamma = 0.7$). In the same figure, as a comparison, the behavior of the median energy of the distribution $A(E) \cdot E^{-\gamma}$ is reported. This could also be used as a definition for the energy threshold, but its dependence on γ, at least for our detector, is much stronger.

Whatever is the chosen definition of E_0, the significance of the upper limits are within $\approx 10\%$ with respect to the assumed primary spectrum.

3.3. Fluxes and upper limits calculations

The number of photons with energy $E > E_0$ detected from a point source with energy spectrum $bE^{-\gamma}$ is:

$$n_\gamma(>E_0) = \epsilon T \int_0^\infty bE^{-\gamma} A(E)\, \mathrm{d}E$$

where ϵ is the angular efficiency (see Table 2) and T the exposure time.

The flux corresponding to n_{oss} observed events is:

$$\Phi_\gamma(>E_0) = \frac{n_{\text{oss}}}{\int_0^\infty E^{-\gamma} A(E)\, \mathrm{d}E} \frac{1}{\epsilon T(\gamma - 1)} E_0^{-\gamma+1}.$$

For internal events S_1 and S_2, for which the effective area A_{eff} is defined, this reduces to:

$$\Phi_\gamma(>E_0) = \frac{n_{\text{oss}}}{\epsilon T A_{\text{eff}}}.$$

The upper limits will be given by calculating n_{oss} at 90% c.l. and following Ref. [31].

4. The results

The searches accomplished on candidate gamma-ray sources are for:

– *DC emission* (on the whole dataset and on one year time scale);

– *sporadic emission*, on a daily transit time scale;

– *time modulated emission*, from sources for which a periodicity is measured at lower frequencies (i.e. $P \approx 4.8$ h for Cygnus X-3, $P \approx 33$ ms for the Crab Pulsar and $P \approx 237$ ms for the Geminga pulsar). The arrival times of individual events are corrected to the barycentre of the solar system using the JPL DE200 ephemeris [32]. This procedure is applied both on source and background events.

Thirteen candidate sources have been studied: they are listed in Table 3 together with their observation parameters and the energy thresholds.

We will discuss in detail the results on Cygnus X-3, the Crab Nebula and Pulsar, and Geminga, and we will summarize the results from the other ones.

4.1. Cygnus X-3

– *DC emission.* Due to the possible source variability, the data have been examined both yearly and globally. For each year and for the total observation time, Table 4 lists the number of observed events, the background ones and the significances of the excesses at the different threshold energies.

There is no evidence of steady emission both in the whole data set and in the yearly ones. The corresponding DC flux upper limits (assuming a source spectrum $\propto E^{-2}$) derived (at 90% c.l.) are shown in Table 4, being e.g.:

$$\Phi(>230\ \text{TeV}) < 2\times 10^{-14}\ \text{cm}^{-2}\ \text{s}^{-1}$$

i.e. $< 1\%$ of the C.R. flux within a solid angle $\Omega = 8\times 10^{-4}$ sr.

– *4.8 h periodic emission*. The X-ray cubic ephemeris by Van Der Klis and Bonnet Bidaud [33] have been used to determine the phase of each event; the data, both ON and OFF, have been assigned to forty phase bins. The light curves have been obtained both for the total period of observation and for each year. No unexpected excess is observed at any phase and at any energy threshold, in any year (the phase plot obtained from the global S_1 data set is shown in Fig. 5). The obtained upper limits to the emission in the bin corresponding to phase 0.625 (at which a signal was reported) are shown in Table 4 (last column).

Table 4
Cygnus X-3: number of events from the source (col. 3), from the background (col. 4), significance of the excess above the background (col. 5), 90% confidence level upper limits to the DC (col. 6) and periodic flux (col. 7)

Year (N_{days})	E_{th} [TeV]	N_{ON}	$N_{\langle\text{OFF}\rangle}$	S	Φ (DC) [$\text{cm}^{-2}\ \text{s}^{-1}$]	Φ (pulse) [$\text{cm}^{-2}\ \text{s}^{-1}$]
1989	25	239146	239483	−0.6	5.9×10^{-13}	9.3×10^{-14}
(104)	90	5727	5705	+0.3	2.9×10^{-13}	4.5×10^{-14}
	230	168	160	+0.6	1.6×10^{-13}	2.5×10^{-14}
1990	25	2614813	2615858	−0.6	3.5×10^{-13}	5.5×10^{-14}
(248)	90	24457	24778	−1.9	5.3×10^{-14}	8.3×10^{-15}
	230	1230	1190	+1.1	3.7×10^{-14}	5.8×10^{-15}
1992	25	1787252	1786923	+0.2	5.6×10^{-13}	8.8×10^{-14}
(225)	90	19782	19512	+1.8	2.1×10^{-13}	3.3×10^{-14}
	230	1113	1112	+0	3.1×10^{-14}	4.9×10^{-15}
1993	25	2323078	2324199	−0.7	3.8×10^{-13}	6.0×10^{-14}
(209)	90	25391	25547	−0.9	6.5×10^{-14}	1.0×10^{-14}
	230	1713	1686	+0.6	2.9×10^{-14}	4.5×10^{-15}
all	25	6964289	6966463	−0.8	1.9×10^{-13}	3.0×10^{-14}
(786)	90	75357	75542	−0.6	4.1×10^{-14}	6.4×10^{-15}
	230	4224	4148	+1.1	2.0×10^{-14}	3.2×10^{-15}

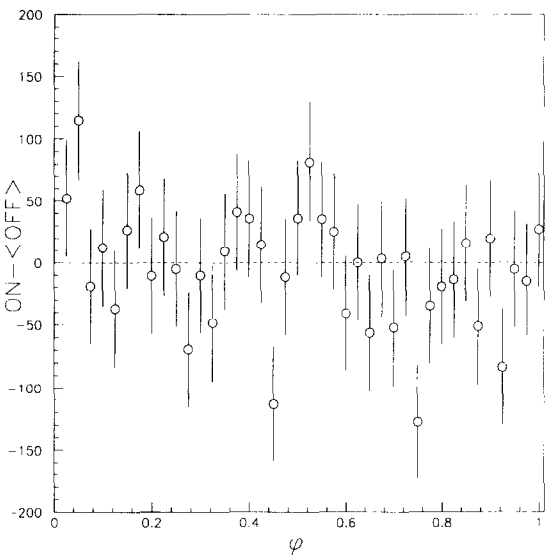

Fig. 5. Cygnus X-3 light curve, obtained from internal events for the total exposure time.

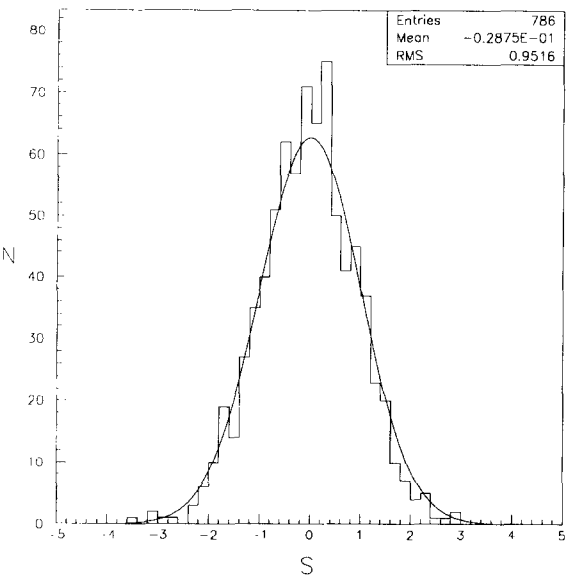

Fig. 6. Distribution of daily excesses for S_1 events from the direction of Cygnus X-3. The expected Gaussian distribution is also shown.

– *Sporadic emission.* Daily excesses significances have been derived and the resulting distributions are for all trigger conditions in optimum agreement with Gaussian ones with mean = 0 and s.d. = 1 (e.g. for S_1 events: $\chi^2 = 35.5$ for $\nu = 49$ degrees of freedom, see Fig. 6). In no case the maximum excess S_{max} measured in 786 days has a probability smaller than 10% to be simulated by background fluctuations. At 90% c.l., < 1.5 events/y have been observed with flux $> \Phi_s$ and duration ≤ 7 h: Φ_s, calculated from S_{max}, is displayed in Table 5.

Table 5
Cygnus X-3: maximum excesses recorded in $N_d = 786$ days of measurements for each data-set, number of events with significance $> S_{max}$ expected in N_d days and the 90% confidence level upper limits to a sporadic emission lasting ≤ 7 h

E_{th} [TeV]	S_{max} [s.d.]	Expected number of events	Φ_s [cm^{-2} s^{-1}]
25	3.8	0.1	1.4×10^{-11}
90	2.9	1.5	2.3×10^{-12}
230	3.7	0.1	8.3×10^{-13}

The obtained upper limits to the DC and periodic fluxes are respectively a factor of almost 80 and 300 lower than the fluxes reported in Refs. [2–4], showing that, during the period 1989–1993, Cygnus X-3 has not been active at the level of early eighties. Moreover, due to the results of the yearly analysis, a long term variation of the emission can be excluded, at least since 1989 to 1993. Lastly, no evidence of significant source activity has been found in any observation day, including those corresponding to radio bursts [34] (June 1989, July 1989, August 1990, October 1990).

Table 6
Crab Nebula and pulsar: summary of the results obtained in the search for DC and pulsed emission (see the caption of Table 3)

N_{days}	E_{th} [TeV]	N_{ON}	$N_{\langle OFF\rangle}$	S	Φ (DC)	Φ (pulse)
816	25	3813499	3813856	−0.2	4.0×10^{-13}	6.9×10^{-14}
	105	41699	41364	+1.5	9.0×10^{-14}	1.6×10^{-14}
	280	2563	2543	+0.4	1.6×10^{-14}	2.8×10^{-15}

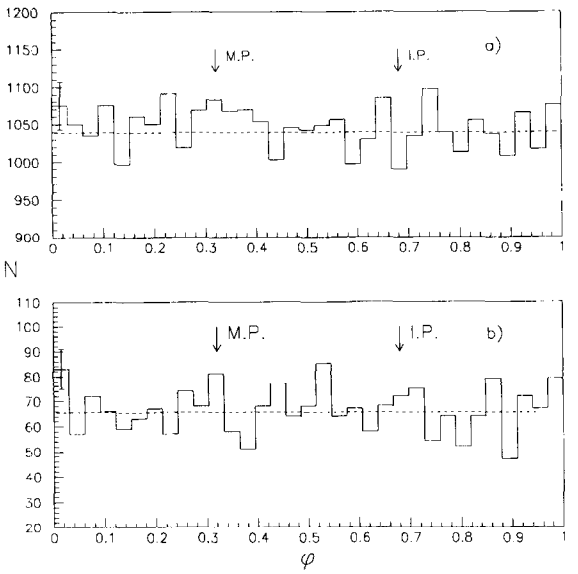

Fig. 7. Crab pulsar light curve, (a): S_1 events, (b): S_2 events. The typical error is shown.

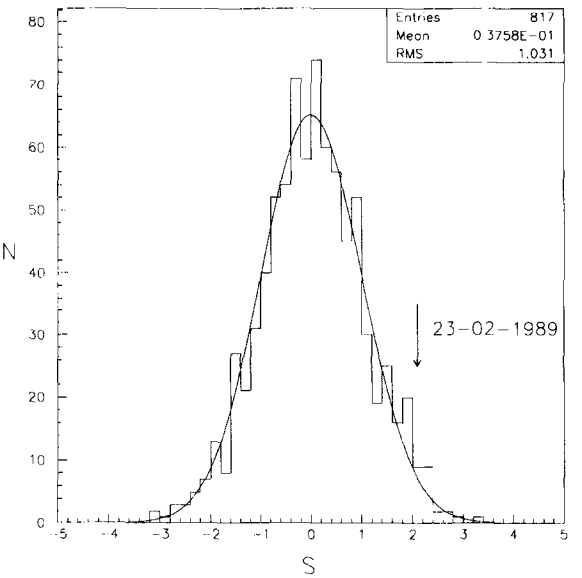

Fig. 8. Distribution of the daily excesses of the S_1 events from the direction of the Crab Nebula. The expected Gaussian distribution is also shown. The arrow indicates the burst of 23 February 1989.

4.2. Crab Nebula and pulsar

– *DC emission.* As it can be seen from Table 6, no evidence for steady emission has been found at any energy threshold. Using a differential energy spectrum $\propto E^{-2.4}$ [5], upper limits to the flux have been obtained: they are reported in Table 6, the one closest to the TeV observations being

$$\Phi\ (>25\ \text{TeV}) < 4\times 10^{-13}\ \text{cm}^{-2}\ \text{s}^{-1}$$

corresponding to $< 0.05\%$ of the cosmic ray flux within a solid angle $\Omega = 0.019$ sr.

– *Pulsed emission.* The ≈ 33 ms pulsar periodicity has been searched by using the Jodrell Bank ephemeris [35]. The events arrival times have been folded into 33 channels phasograms: Figs. 7a and 7b show such light curves obtained with S_1 and S_2 events respectively (the phases of optical pulses, main and interpulse, are indicated). No channel shows unexpected excesses: the upper limits to the emission in the bin corresponding to the main pulse ($\Delta t = 1$ ms) have been derived and are reported in last column of Table 6.

– *Sporadic emission.* No unexpected excess is observed in any daily excess distribution: such distribution for S_1 events is shown in Fig. 8, being its $\chi^2 = 40$ for $\nu = 49$ d.o.f. with respect to a reduced Gaussian (also shown in the figure). The derived flux limits Φ_s are presented in Table 7: at 90% c.l., less than 1.5 events/y have been observed with a flux $> \Phi_s$ and duration $\leqslant 5.5$ h (for a similar search concerning the epoch since 1982 to 1086 see Ref. [36]).

The study of transient phenomena through contemporaneous observations by different arrays is thus most important. Of particular significance is the burst recorded on 23rd February 1989 from

Table 7
Crab Nebula: maximum recorded excesses in $N_d = 816$ days of measurements for each data-set, number of events with significance $> S_{max}$ expected in N_d days and the 90% confidence level upper limits to a sporadic emission lasting ≤ 5.5 h

E_{th} [TeV]	S_{max} [s.d.]	Expected number of events	Φ_s [$\text{cm}^{-2}\ \text{s}^{-1}$]
25	2.6	3.8	2.1×10^{-11}
105	3.2	0.6	2.7×10^{-12}
280	3.2	0.6	7.7×10^{-13}

Table 8
Summary of the observations of the Crab Nebula on the 23rd February 1989, by the Baksan, KGF and EAS-TOP arrays

Array	Time (UT)	ON	⟨OFF⟩	S
KGF	13–16	35	17.8	3.4
Baksan	15–18	55	34.1	3.1
EAS-TOP (S_1)	17–20	38	25.5	2.1
EAS-TOP (S_3)	17–20	403	378.3	1.2

the direction of the Crab Nebula by the Baksan [6], KGF [7] and EAS-TOP [8] arrays. The three experiments detected an excess of showers, at the transit times of the Crab Nebula over them: a summary of the three observations is given in Table 8.

The significance of the event recorded by the EAS-TOP array alone is 2.4 s.d. (the excess found in S_1 events is shown in fig. 8) and the observed flux in ≈ 5.5 h of observation is

$$\Phi\ (>105\ \text{TeV}) = 2 \pm 1 \times 10^{-12}\ \text{cm}^{-2}\ \text{s}^{-1}.$$

We use the same energy threshold as for the DC limits, although the photon energy spectrum in the burst could be different; the used definition is in fact rather independent from the energy spectrum (see Section 3.2).

This event, which has a total probability of being simulated by background fluctuations $\approx 10^{-5}$, still stands as the most significant excess recorded at UHE energies.

4.3. Geminga

– *DC emission.* The results of a search for a DC excess are summarized in Table 9.

No statistically significant excess has been detected; the derived upper limits to the flux (source spectrum $\propto E^{-2}$) are shown in the same table, being e.g.:

$$\Phi\ (>40\ \text{TeV}) < 2.4 \times 10^{-13}\ \text{cm}^{-2}\ \text{s}^{-1}$$

corresponding to 0.05% of the cosmic ray flux within 0.019 sr.

– *Pulsed emission.* Following the observation of a pulsed signal, with a period of ≈ 0.237 s, both in X-rays [37] and in 300 MeV gamma-rays [10], a pulsed UHE gamma-ray emission has been searched in the EAS-TOP 1992 and 1993 datasets. The position of the X source G″ (R.A. = 6h 33m 54.02s, DEC. = +17°46′11″ in 2000 [38]) and the EGRET ephemeris [39–40] have been used. The uncertainties on such ephemeris make possible to fold the arrival times into a 20 bins light curve for our whole observation time, the binning being decided a priori so that the phase of EGRET "peak 1" coincides with the center of one of them.

First results based on ≈ 1200 h of observation since December 1991 to January 1993 have been presented in Ref. [41]. The S_3 events (which showed a slight excess at 1.5 s.d.) were subjected to a periodic analysis using the pulsar ephemeris given in [39]: the resulting light curve showed 2.5 and 3.1 s.d. excesses in the two bins corresponding to the phases of EGRET peak 1 and peak 2. Including the fact that four data sets were searched, the overall imitation rate of the excess resulted to be 2×10^{-4}.

The observation time has now increased to ≈ 2200 h, extending until December 1993: Table 10 shows the collected number of counts together with their significances, for all the trigger conditions.

The S_3 data set still presents a slight d.c. excess at 1.7 s.d.: the arrival time of each event has been folded using the most recent pulsar

Table 9
Geminga: summary of the DC data for the complete database (1989–1993)

N_{days}	E_{th} [TeV]	N_{ON}	$N_{\langle\text{OFF}\rangle}$	S	Φ (DC)
811	40	2864546	2863202	+0.7	2.4×10^{-13}
	140	30948	30969	−0.1	5.0×10^{-14}
	350	1319	1310	+0.2	1.8×10^{-14}

Table 10
Geminga: summary of the DC data collected in 1992 and 1993

E_{th} [TeV]	N_{ON}	$N_{\langle\text{OFF}\rangle}$	S
30	586783	586724	+0.1
45	1045655	1043798	+1.7
140	19128	19051	+0.5
350	1319	1311	+0.2

Table 11
Geminga: maximum recorded excesses in $N_d = 811$ days of measurements for each data-set, number of events with significance $> S_{max}$ expected in N_d days and the 90% confidence level upper limits to a sporadic emission lasting ≤ 5.5 h

E_{th} [TeV]	S_{max}	Expected number of events	Φ_s [cm^{-2} s^{-1}]
40	3.2	0.6	1.0×10^{-11}
140	2.7	2.8	2.3×10^{-12}
350	2.8	2.1	6.5×10^{-13}

ephemeris [40]. The obtained light curve is shown in fig. 9: the two arrows indicate the phases of peak 1 (P1) and peak 2 (P2). The light curve shows only one excess in the bin corresponding to peak 1: it contains 52 971 events while 52 190 are expected from a uniform distribution of the background into the 20 bins, corresponding to an excess of 3.4 s.d.

Taking into account the total number of data sets analyzed (4) and the number of peaks of the

Table 12
Results obtained in the search for DC emission through the complete database (1989–1993) from the 10 candidate sources

Source (N_{days})	E_{th} [TeV]	N_{ON}	$N_{\langle OFF\rangle}$	S	Φ (DC) [10^{-14} cm^{-2} s^{-1}]
Hercules	25	6382512	6387242	−1.7	12
X-1	90	69515	69312	+0.7	6.8
(800)	240	4025	3967	+0.9	1.9
Cygnus	25	3711293	3712610	−0.6	21
X-1	90	40473	40733	−1.2	4.2
(437)	240	2629	2607	+0.4	1.9
4U0	25	5280196	5273043	+2.9	60
115 + 6112	120	54801	54682	+0.5	5.5
(738)	300	1811	1780	+0.7	1.7
PSR	25	5222050	5224898	−1.2	16
1953 + 29	100	56695	56812	−0.5	4.5
(800)	260	2228	2215	+0.3	1.9
PSR	25	3659668	3662983	−1.6	15
1937 + 214	120	39614	39814	−0.9	3.7
(810)	300	1622	1630	−0.2	1.6
PSR	25	3213713	3211822	+1.0	42
0157 + 6112	120	34104	34101	+0.02	5.8
(408)	300	1981	1919	+1.3	2.2
LSI + 61	25	3345589	3345253	+0.2	32
(410)	120	35673	35676	−0.01	5.8
	300	1978	2010	−0.7	1.1
North Gal.	25	4882259	4881099	+0.5	3.2
Pole	100	52896	52719	+0.7	6.9
(808)	260	2120	2156	−0.7	1.3
M31	25	7021155	7024759	−1.3	14
(780)	90	75467	75922	−1.5	3.0
	230	2714	2776	−1.1	1.1
Markarian	25	3996585	4002534	−2.8	11
421	90	43654	43903	−1.1	4.4
(441)	240	2770	2841	−1.2	1.1

emission (2), the overall imitation rate is 2×10^{-3}. This is not low enough to allow a definite conclusion; therefore we derive the 90% c.l. upper limit to the pulsed emission in the two pulsar peaks:

Φ (> 45 TeV) < 1.2×10^{-13} cm^{-2} s^{-1}.

– *Sporadic emission.* All the excess distributions are well described by a reduced Gaussian behavior (χ^2 is 39 with $\nu = 49$ for S_1 events, see Fig. 10) and no unexpected excess has been found. The derived flux limits shown in Table 11 give < 1.5 events/y (at 90% c.l.) with a flux > Φ_s and duration ≤ 5 h.

4.4. Other candidate sources

Ten other candidate point sources have been examined (Table 12 shows the number of days of observation ON source and the total number of collected events).

– *Long term emission.* No statistically significant d.c. excess has been found from any of the observed sources, at any energy threshold: Table 12 shows the results and the 90% c.l. upper limits (assumed source spectra $\propto E^{-2}$).

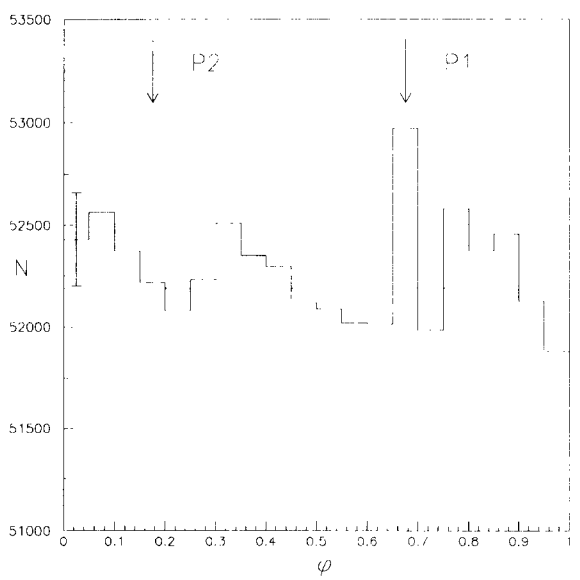

Fig. 9. Geminga Pulsar light curve. Phases corresponding to peak 1 (P1) and 2 (P2) of "EGRET" emission are indicated. The typical error is shown.

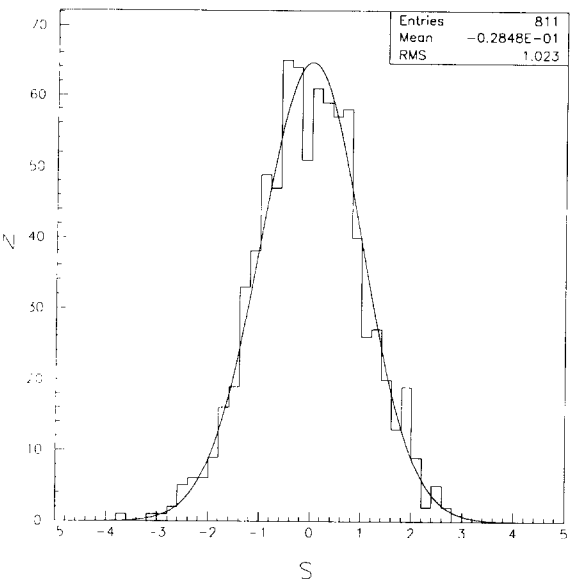

Fig. 10. Distribution of the daily excesses of the events from the direction of Geminga, together with the expected Gaussian distribution.

– *Sporadic emission.* We discuss more in detail the observations of Hercules X-1, in the past reported as a sporadic UHE emitter (see e.g. Ref. [42]): the distribution of the daily excesses in the direction of Hercules X-1 is shown in Fig. 11 for S_1 events (where the comparison with a reduced Gaussian distribution gives $\chi^2 = 25$ for $\nu = 49$). No unexpected excess have been recorded at any energy threshold: the 90% c.l. upper limit gives a rate < 1.1 events/y with flux > Φ_s and duration ≤ 7 h. The results of the analysis are given in Table 13, for all the investigated candidate sources. All the maximum observed excesses are compatible with the expectations: also events with probabilities of chance imitation ≈ 10^{-2}–10^{-1} (as for Markarian 421 and PSR 1937 + 214) are not significant, due to the number of channels analyzed.

5. Conclusions

We have presented the results obtained from four years (1989–1993) of systematic observations of the EAS-TOP e.m. detector in the search for

UHE gamma-ray emission from candidate point sources observable in the northern hemisphere.

The detector angular resolution is $\sigma_\vartheta \approx 0.83°$ at energy $E_0 \approx 100$ TeV ($\approx 0.5°$ at ≈ 250 TeV): this is checked for each successive year of operation through the measurement of the shadowing effect on the cosmic rays flux by the Moon. Moreover, the counting rate stability has been systematically monitored, the upper limit to the level of instabilities being $< 0.08\%$.

Thirteen sources have been studied concerning possible DC, sporadic and periodic emission: no evidence for significant excess has been found and upper limits have been placed.

In the case of Cygnus X-3, the limits (e.g. Φ_{DC} (> 230 TeV) $< 2.0 \times 10^{-14}$ cm^{-2} s^{-1}, $\Phi_{4.8h}$ (> 230 TeV) $< 3.2 \times 10^{-15}$ cm^{-2} s^{-1}) are well below the fluxes reported in early eighties (a factor ≈ 80 and ≈ 300 respectively for DC and periodic signals). Moreover, a long term variation in the

Table 13
Maximum daily recorded excesses for the total exposure time, expected number of events with significance $> S_{max}$ and 90% upper limits to sporadic emission for 10 candidate sources (the daily observation time is shown in Table 3 for each source)

Source	E_{th} [TeV]	S_{max} [s.d.]	Expected number of events	Φ_s [cm^{-2} s^{-1}]
Hercules X-1	25	3.0	1.0	1.2×10^{-11}
	90	3.3	0.4	2.7×10^{-12}
	240	2.9	1.5	6.7×10^{-13}
Cygnus X-1	25	2.3	4.7	8.1×10^{-12}
	90	2.7	1.5	2.0×10^{-12}
	240	2.8	1.1	6.0×10^{-13}
4U0 115 + 6112	25	3.3	0.4	1.2×10^{-11}
	120	2.9	1.4	2.0×10^{-12}
	300	3.6	0.1	6.1×10^{-13}
PSR 1953 + 29	25	2.8	2.1	1.1×10^{-11}
	100	2.9	1.5	2.4×10^{-12}
	260	2.7	2.8	6.1×10^{-13}
PSR 1937 + 214	25	3.5	0.2	1.6×10^{-11}
	120	4.5	0.01	3.7×10^{-12}
	300	3.4	0.3	7.8×10^{-13}
PSR 0157 + 6112	25	3.2	0.3	1.1×10^{-11}
	120	2.7	1.4	1.8×10^{-12}
	300	2.9	0.8	5.1×10^{-13}
LSI + 61	25	2.6	1.9	9.4×10^{-12}
	120	2.3	4.4	1.6×10^{-12}
	300	2.6	1.9	4.6×10^{-13}
North Gal. Pole	25	3.3	0.4	1.3×10^{-11}
	100	2.9	1.5	2.4×10^{-12}
	260	3.5	0.2	8.1×10^{-13}
M31	25	2.6	3.7	9.8×10^{-12}
	90	3.5	0.2	2.9×10^{-12}
	230	2.6	3.7	5.5×10^{-13}
Markarian 421	25	3.7	0.1	1.3×10^{-11}
	90	3.3	0.2	2.6×10^{-12}
	240	2.7	1.5	6.0×10^{-13}

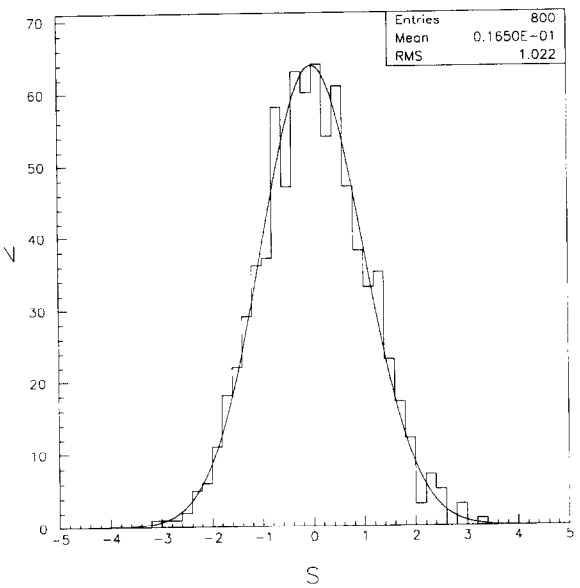

Fig. 11. Distribution of the daily significances of the events from the direction of Hercules X-1, and the expected Gaussian distribution.

emission can be excluded, due to the yearly analysis, at least since 1989 to 1993.

The upper limits obtained from the Crab Nebula are at the level of the extrapolation of the measured $0.5 \div 5$ TeV flux to the energy region around 30 TeV (Φ (> 25 TeV) $< 4 \times 10^{-13}$ cm^{-2} s^{-1}). The results obtained in the search for sporadic emission is negative at a flux level $\approx 2.7 \times 10^{-12}$ cm^{-2} s^{-1} at energies > 105 TeV and for a duration ≈ 5 h. The only significant positive sporadic excess is still the burst detected by the EAS-TOP, Baksan and KGF arrays on 23 February 1989, for which the overall confidence level is $\approx 10^{-5}$. The corresponding flux is about 60 times higher than the extrapolation at 100 TeV of the observed TeV flux, with probable duration ≈ 10 h.

Of some particular interest is the results of the search for a periodic signal (237 ms) from Geminga: the light curve shows a 3.4 s.d. excess in the bin corresponding to the EGRET higher peak. The associated probability for the effect to be simulated by a background fluctuation is $\approx 2 \times 10^{-3}$: being not compelling for the identification of a signal, an upper limit to the pulsed emission at the phases of the two pulsar peaks is: $\Phi(> 45 \text{ TeV}) < 1.2 \times 10^{-13}$ cm^{-2} s^{-1}.

Acknowledgments

The authors wish to thank the Director of the Laboratori Nazionali del Gran Sasso and all the laboratory staff for their constant support. Thanks are also due to C. Barattia, R. Bertoni, M. Canonico, G. Giuliani, A. Giuliano, G. Pirali for their continuous technical assistance.

A stimulating discussion with J. Cronin is gratefully acknowledged.

References

[1] Y.I. Nesphor et al., Astrophys. Space Sci. 61 (1979) 349.
[2] C. Morello et al., Proc. 18th Int. Cosmic Ray Conf., Bangalore, August 1983, 1, 137;
C. Morello et al., Il Nuovo Cimento 13C (1990) 453.
[3] M. Samorsky and W. Stamm, Ap. J. 268 (1983) L17.
[4] J. Lloyd-Evans et al., Nature 305 (1983) 784.
[5] G. Vacanti et al., Ap. J. 377 (1991) 467.
[6] V.V. Alexeenko et al., J. Phys. G 18 (1992) L83.
[7] M. Acharya et al., Nature 347 (1990) 364.
[8] M. Aglietta et al., Europhysics Lett. 15 (1991) 81.
[9] D.L. Bertsch et al., Ap. J. Lett. 415 (1993) 113.
[10] D.L. Bertsch et al., Nature 357 (1992) 306.
[11] C.C.G. Bowden et al., J. Phys. G 19 (1993) L29.
[12] P.R. Vishwanath et al., Astron. Astrophys. 267 (1993) L5.
[13] C.W. Akerlof et al., Astron. Astrophys. 274 (1993) L17.
[14] M. Punch et al., Nature 358 (1992) 447.
[15] M. Aglietta et al., Nucl. Instr. Meth. A 277 (1988) 23.
[16] M. Aglietta et al., Nucl. Instr. Meth. A 336 (1993) 310.
[17] M. Aglietta et al., Proc. 21st Int. Cosmic Ray Conf., Adelaide, January 1990, Vol. 2, 345.
[18] M. Aglietta et al., Proc. 22nd Int. Cosmic Ray Conf., Dublin, August 1991, Vol. 1, 277.
[19] M. Aglietta et al., Proc. 23rd Int. Cosmic Ray Conf., Calgary, August 1993, Vol. 1, 216.
[20] M. Aglietta et al., Proc. 22nd Int. Cosmic Ray Conf., Dublin, August 1991, Vol. 1, 404.
[21] M. Aglietta et al., Ap. J. 397 (1992) 148.
[22] D.E. Alexandreas et al., Ap. J. 383 (1991) L53.
[23] J.W. Cronin et al., Phys. Rev. D 45 (1992) 4385.
[24] M. Amenomori et al., Phys. Rev. Letts. 69 (1992) 2468.
[25] M. Merck et al., Proc. 23rd Int. Cosmic Ray Conf., Calgary, August 1993, Vol. 1, 361.
[26] M. Aglietta et al., Proc. 22nd Int. Cosmic Ray Conf., Dublin, August 1991, Vol. 2, 708.
[27] T. Li and Y. Ma, Ap. J. 272 (1983) 317.
[28] C. Forti et al., Phys. Rev. D 42 (1990) 3668.

[29] M. Aglietta et al., Proc. 23rd Int. Cosmic Ray Conf., Calgary, August 1993, Vol. 4, 247.
[30] K. Kamata et al., Prog. Theor. Phys. Suppl. 6 (1958) 93.
[31] O. Helene, Nucl. Instr. Meth. 212 (1982) 319.
[32] E.M. Standish, Astron. Astrophys. 114 (1982) 297.
[33] M. Van Der Klis and J.M. Bonnet Bidaud, Astron. Astrophys. 214 (1989) 203.
[34] K. Johnston, private communication (1989).
[35] A.G. Lyne and R.S. Pritchard, private communication (1994).
[36] C. Morello et al., Il Nuovo Cimento C10 (1987) 142.
[37] J.P. Halpern and S.S. Holt, Nature 357 (1992) 222.
[38] J.P. Halpern and D. Tytler, Ap. J. 330 (1988) 201.
[39] H.A. Mayer-Hasselwander, IAU Circular no. 5649 (1992).
[40] J. Mattox et al., 1994. Proc. 2nd Compton Gamma-Ray Observatory Symposium, College Park, MD, Sept. 20–22 1993, AIP, in press.
[41] M. Aglietta et al., Proc. 23rd Int. Cosmic Ray Conf., Calgary, August 1993, Vol. 1, 309.
[42] B.L. Dingus et al., Phys. Rev. Letts. 61 (1988) 1906.